

Molecular Modeling of Protein Structure, Biology of Disease and Clinical Electroretinography in Human X-Linked Retinoschisis (XLRS)

Yuri V. Sergeev¹, Kristen E. Bowles¹,
Lucia Ziccardi² and Paul A. Sieving^{1,2}

¹*Ophthalmic Genetics and Visual Function Branch, National Eye Institute*

²*Section of Translational Research in Retina & Macular Degeneration*

National Institute on Deafness and Other Communication Disorders

*National Institutes of Health, Bethesda, Maryland
USA*

1. Introduction

We describe a promising approach using *in silico* structure-function studies of protein atomic structure and computational medicine to understand disease. *In silico* studies use an atomic structure of proteins and molecular modeling for structure-function analysis. This approach is critical for large-scale genetic studies in order to understand a possible functional role of genetic mutations. Indeed, structural changes associated with missense mutations might impact protein folding, protein-protein interaction sites, or solubility or stability of protein molecules. The structural effect of mutational changes can be analyzed *in silico* on the basis of 3-dimensional structure, multiple alignments of homologous sequences, molecular modeling, and molecular dynamics simulations. The parameters derived from 3-dimensional protein structure could be used in clinical studies to predict a severity of protein structure-function changes caused by genetic mutations and evaluate genotype-to-phenotype relationships. In this chapter, we use X-linked retinoschisis (XLRS) as our disease model. XLRS is a form of juvenile macular and retinal degeneration in which schisis or splitting within the retinal layers leads to early and progressive vision loss. XLRS is a rare disease estimated to affect 1:5000 males (George et al., 1995; Wang et al., 2002) and is a disease with considerable clinical and electrophysiological variation. Precise analysis of XLRS is pertinent to identify disease severity and genotype-phenotype correlation. Due to the lack of a protein assay, a correlation between phenotype and genotype is difficult. Advances in molecular modeling give new insight to mutation severity at atomic level and provide a possible connection between genotype-phenotype correlations. This creates the hope that disease risk assessment at the atomic level will be a reality in the future. For our study, we use the electroretinogram (ERG) for our phenotypical data set, which we correlated with expected mutation severity.

2. Biological factors and electroretinography of XLRS

2.1 Biology of retinoschisin protein: secretion and expression, hypothesized function, underlying mechanisms of functional loss of RS1 protein

Retinoschisin (RS1) is a retinal secreted photoreceptor disulphide-linked oligomeric protein. A number of mutations in RS1 co-segregate with XLRS providing strong evidence that the disease is caused by mutations in the *RS1* gene (Sauer et al., 1997). Although inherited mutations in the *RS1* gene have been shown to cause an XLRS phenotype, the functional impact of most missense variants that result in a single amino acid change is less well defined. RS1 is a 24-kDa secreted protein which is expressed exclusively in the retina (Reid et al., 1999), pineal gland (Takada et al., 2006), and uterus (Huopaniemi et al., 1999). In retinal layers it is found in photoreceptor cells and in neurons of the inner retina (Figure 1). It encodes a conserved discoidin domain homologous to proteins involved in cell adhesion and cell-cell interactions. Based on its structural features, RS1 is believed to hold retinal cells together, to preserve the retinal architecture, and to function as an adhesive protein for the structural and functional integrity of the retina (Molday et al., 2007; Vijayasarathy et al., 2007). It may mediate the association of the extracellular matrix with the surface of photoreceptors and other retinal cells to promote cell adhesion and thereby stabilize the cellular architecture of the highly structured retinal tissues. There exist three primary mechanisms that may be responsible for the loss of function of the RS1 protein: the misfolding of the discoidin domain, which negatively influences the putative adhesive properties of the protein; the defective disulfide-linked subunit assembly of RS1 into dimers and octamers; or the inability of RS1 to insert into endoplasmic reticulum membrane as part of the protein secretion process.

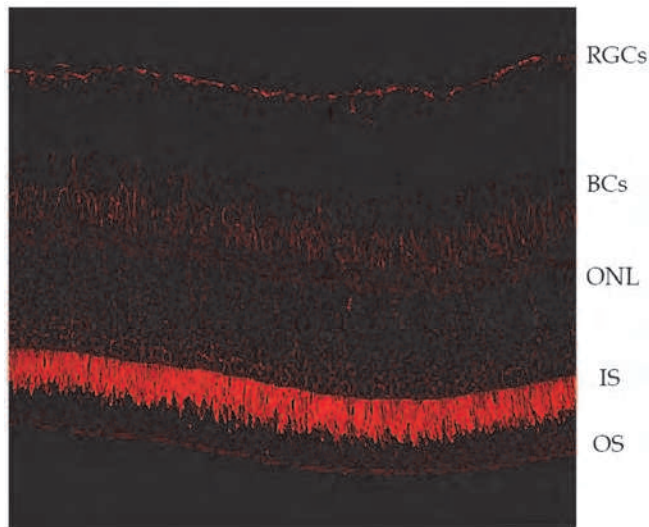


Fig. 1. RS1 labeling in a wild-type mouse. Immunohistochemistry with antibody raised against RS1 protein. RS1 labeling in a normal adult C57BL/6J mouse retina, displayed by confocal microscopy, is observed in all retinal layers. On the right are shown RGCs: retinal ganglion cells, BCs: bipolar cells, ONL: outer nuclear layer, IS: inner segments, OS: outer segments.

2.2 Retinal morphology in retinoschisis: photoreceptors disruption and altered photoreceptor/bipolar cells synapse in the RS1-KO mouse

Currently, there are three mouse models of human XLRs. One has been generated by homologous DNA insertion across the endogenous *RS1* gene (Weber et al., 2002), presenting a phenotype consisting of abnormal retinal architecture with schisis in the inner nuclear layer, reduced outer segment layer thickness, loss of photoreceptors, and a selective ERG b-wave reduction with relative sparing of the a-wave similar to XLRs male subjects. A second *RS1* knock-out mouse model (Zeng et al., 2004) was created by substituting a neomycin resistance cassette for exon 1 and 1.6 kb in intron 1 of *RS1h*, the murine orthologue of the human *RS1* gene. This model also displayed structural and functional features similar to those of human XLRs, including the electronegative ERG waveform and splitting in the inner nuclear layer similar to retinoschisis cavities by 6 months of age. They also demonstrated displacement of cells from the photoreceptor outer nuclear layer (ONL) and reduced thickness of the outer segment layer (Zeng et al., 2004). More recently, a third mouse model was generated using an ENU mutagenesis approach (Jablonski et al., 2005) derived from an induced mutation in intron 2 of *RS1h*, which leads to two novel splice variants. It is remarkable that, similar to the human condition, male homozygous mutant mice have retinal abnormalities as early as two weeks of age which do not appear to progress up to 38 weeks.

2.3 Clinical features of XLRs disease: visual acuity, visual field, OCT, fundus appearance, ERG

XLRs classical phenotype is present in two-thirds or more of affected males (George et al., 1996) and consists in an early-onset central vision loss from bilateral foveo-macular cystic cavities involving the inner retina and additional retinal layers (Gregori et al., 2009) that extend from the fovea in a spoke-wheel pattern for approximately 1-1.5 disc diameter (Figure 2).

XLRs patients often have hyperopic refractive error with astigmatism (Roesch et al., 1998; Kato et al., 2001; Vijayasarathy et al., 2009). Visual acuity ranging between 20/20 to 20/200 in young patients, who come to ophthalmological attention because of reading difficulty, due to the macular involvement of the disease. Patients typically exhibit modest severity at a young age (cystic form), with a slow progression until the second decade, when most retain around 20/70 vision. It worsens through the teenage years and stabilizes in adulthood when the atrophic stage can lead to legal blindness (Lesch et al., 2008). However, some XLRs males exhibit unpredictable, severe disease even at very early age, and surprisingly, the ERG can show an unexpected preservation of the scotopic b-wave (Eksandh et al., 2005; Sieving et al., 1999a).

XLRs is a highly penetrant disease condition (Forsius et al., 1973). In some cases subtle retinal changes are difficult to identify by ophthalmoscopy and can be detected only by optical coherence tomography (OCT) scans (Eriksson et al., 2004) (Figure 2). In the late stages of the disease when macular atrophy starts, a hyperfluorescent window defect of the retinal pigment epithelium (RPE) on fluorescein angiography (FA) can be observed. This feature, however, can mimic retinal abnormalities seen in age-related macular degeneration or Stargardt maculopathy. In such cases, the combination of ERG, FA, and OCT is needed to determine the correct diagnosis. The electronegative scotopic ERG is pathognomonic of XLRs; the FA will not exhibit the dark choroid sign that is typically present in Stargardt's maculopathy; and the OCT can detect cysts otherwise undetectable by standard

ophthalmoscopy. Peripheral retinoschisis can be found in half of affected males. Retinal splitting can involve all the retinal layers through the nerve fiber layer. The consequent abnormal visual signaling causes an dense scotoma in the involved areas (Li et al., 2007). Sometimes peripheral retinal scars, possibly to be considered pre-existing areas of self-limited schisis, can be observed.

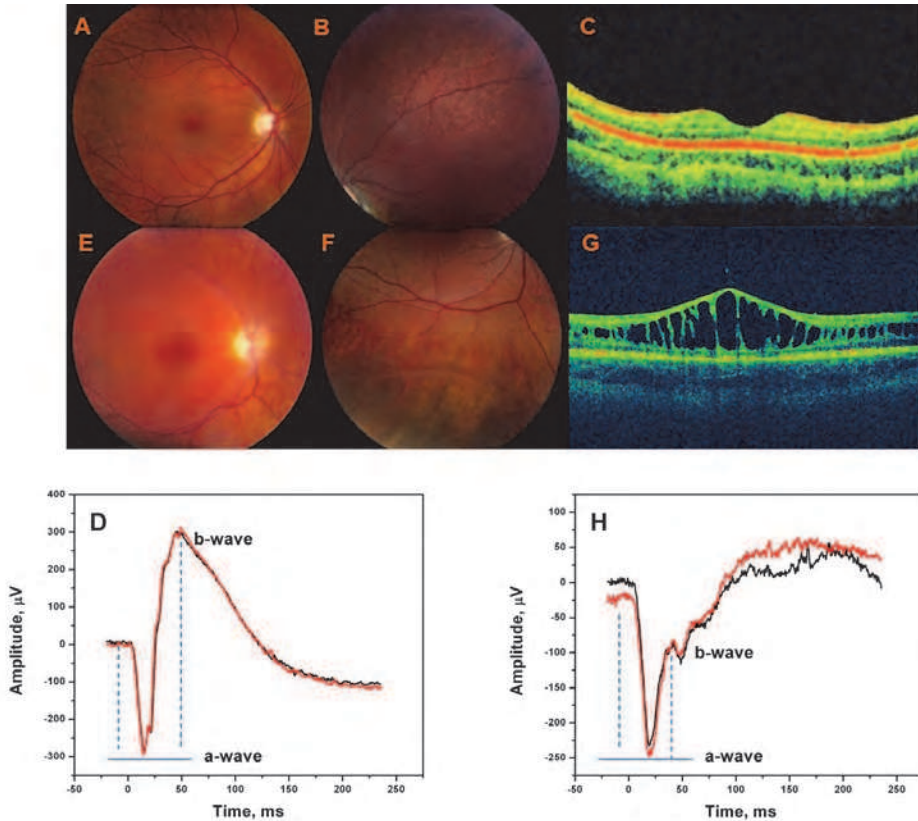


Fig. 2. Collage of Prototypical Fundus (A, B, E, F), OCT (C, G) and ERG (D, H) in normal and in affected by XLRS individuals. Panels A-D and E-H correspond to the normal and the XLRS affected individuals, respectively.

2.4 Photoreceptor and bipolar cell function as seen in the full field ERG

The ERG is a useful tool for evaluate outer retinal function and may assist in identifying the primary sight of XLRS pathology. Through the interpretation of the ERG, one can pinpoint disease at the cellular level in outer retinal visual loss and monitor disease progression. The ERG is a good phenotypical measurement in wide spread disease due to its objective nature and ability to measure function of the entire retina. To better understand the pathology behind the characteristic electronegative ERG in XLRS, one must first understand normal retinal physiology. In a dark-adapted retina, free flowing ions move to and from the rod

photoreceptor. When rhodopsin in the rod photoreceptor captures a photon of light, it undergoes a conformational change causing a cascade of intracellular events within the photoreceptor outer segment resulting in hyperpolarization of the cell. Rod hyperpolarization causes an increased ionic potential towards the distal retina that results in the a-wave (Breton et al., 1994; Hagins et al., 1970). The rod then signals the on-bipolar cell which depolarizes and causes an influx of ions into the proximal retina. This forms the ERG b-wave. In XLR5, the b-wave amplitude is smaller than the a-wave amplitude (i.e. does not return to pre-flash baseline) and is deemed 'electronegative' (Figure 2H). An electronegative ERG suggests dysfunction proximal to the rod outer segment.

2.5 Bipolar cell dysfunction and “electronegative” b-wave in both human and murine model of XLR5

In the retina of the RS1-deficient mouse and the XLR5 human the reduced scotopic ERG b-wave amplitude (Figure 2H) suggests an effect on bipolar-cell function, perhaps initiated from an altered photoreceptor/bipolar-cell synapse activity. This implies primary involvement of the inner retina where schisis cavities occur in XLR5. The identification of L-type voltage-gated calcium channels (Shi et al., 2009), Na/K ATPase (alpha3, beta2 isoforms) (Friedrich et al.), the sterile alpha and TIR motif-containing protein SARM1 (Molday, 2007), and phospholipids/Ca²⁺ (Vijayasarathy et al., 2007) as potential RS1 interacting ligands corroborate a role for RS1 in cell signaling events as well. However, ERG show considerable variation in this disease and ophthalmologists have to be aware about the possibility of relative ERG b-wave preservation especially in presence of atypical or mild manifestation of the disease (Eksandh et al., 2005; Sieving et al., 1999a; Vijayasarathy et al., 2009). These observations may imply that the degree of ERG dysfunctions may not correlate with the extent of fundus involvement and that synaptic integrity might be impaired secondarily over a greater extent of the fundus. In addition, because disruption of the inner segment architecture due to the loss of RS1 might be the basic mechanism that underlies the displacement and disorganization of photoreceptors in RS1-deficient mouse retina, reduced ERG a-wave responses can be found (Kjellstrom et al., 2007b). Clinically, abnormal photoreceptor function has been described in some XLR5 subjects (Bradshaw et al., 1999; Kellner et al., 1990) mostly related to the advanced stages of the disease (Peachey et al., 1987) when the outer retinal atrophy may occur.

2.6 The significance of phenotypic b/a-wave ratio

In retina electrophysiology signal transmission between rod photoreceptors and the post-synaptic bipolar cell neurons is measured by the amplitudes of the a-wave and b-wave, respectively (Newman and Odette, 1984; Robson and Frishman, 1995; Stockton and Slaughter, 1989). To account for any compromise of the photoreceptor layer in XLR5, a ratio of photoreceptor to bipolar-cell synaptic transmission compared to photo-transduction quality can be used: the b-wave amplitude to a-wave amplitude ratio (b/a-wave ratio). One can use the b/a-wave ratio to adjust for any photoreceptor dysfunction affect on the b-wave amplitude, and can imply the quantity of dysfunction in bipolar cells. Normally the b-wave amplitude is greater than the a-wave in the dark-adapted ERG for bright stimuli, but in XLR5 the b-wave naturally is reduced (Peachey et al., 1987). Thus, a reduced b/a-wave ratio is characteristic of inner retinal disease such as XLR5.

2.7 Natural history and disease progression: role of age

Several reports based on visual acuity loss (Apushkin et al., 2005), fundus changes with schisis cavities modification (Lesch et al., 2008), and retinal function deterioration (Vijayasarathy et al., 2010; Vijayasarathy et al., 2009) have focused on the “progressive” nature of XLRS disease. In detail, visual acuity is mostly impaired starting in grade school (Apushkin et al., 2005) due to macular schisis. However, even if 20% of XLRS children (Roesch et al., 1998) present significant vision loss in early childhood, half of these patients may have poor vision due to complications of the disorder, such as retinal detachment or vitreous hemorrhage. A bimodal age is a characteristic of presentation of XLRS in childhood (George et al., 1996). One group presented strabismus and nystagmus at an age less than 2 years, and the other group presented only poor vision at approximately 7 years of age. Exotropia and esotropia were in the same proportion, and in the group with exotropia the occurrence of poor vision from severe schisis was highest. Rhegmatogenous (tractional retinal detachment) may also be the initial presentation of XLRS. Other XLRS males may present during infancy peripheral bullous elevation of the inner retinal layer accompanied with vitreous hemorrhage (George et al., 1996). In such cases it is difficult to assess a “progressive” trait of the disease.

Retinal appearance at funduscopy, OCT scans and ERG b-wave amplitude reduction (Figure 2, E-H) provide an estimate of the retinal changes in XLRS patients. A substantial change from the “cystic” (< 25 years old) to the “atrophic” (> 25 years old) pattern of the retina with age was recently described (Lesch et al., 2008). We also showed (Vijayasarathy et al., 2009) worsening of retinal function by age in a family harboring a null mutation in exon 5 of the *RS1* gene indicating disease progression with age. In this study, the two younger males, ages 1.5 and 5 years, had well preserved b-waves extending above the pre-flash baseline and nearly normal ERG a-wave and b-wave configuration with a classical XLRS fundus appearance. However, four older affected male relatives, ages 32, 43, 43, and 48 years, showed the classic “electronegative” ERG with advanced XLRS retinal changes with reduced electronegative, b-waves. This suggests that older subjects had markedly decreased b-wave amplitudes compared to the younger subjects.

In addition, disease progression has also been observed in natural history studies of the *RS1* knockout-mouse model (Kjellstrom et al., 2007b): progressive loss of photoreceptor nuclei and shortening of the outer segments with age has been found with a considerably reduction of the ERG a-wave amplitude by 16 months. An exact understanding of how XLRS disease progresses with age is not clear. In a recent study (Kjellstrom et al., 2010), 10 XLRS subjects underwent baseline ERG testing between the ages of 6 and 15 years. Follow up ERG testing was performed 8 to 14 years later. For the cohort, no difference was found either between the b-wave amplitude or b/a-wave ratio from the first to second visit.

2.8 Clinical severity (metaanalysis of severity grade systems) and genotype-phenotype correlation in human XLRS

Wide phenotypic heterogeneity is one of the remarkable characteristic of this disease, and it is possibly related to the increasing number of mutations identified in the *RS1* gene (1998). Currently, there is no standard method to grade the severity of XLRS disease. The clinical presentation of XLRS patients can vary based on the age of patients. Strabismus, nystagmus, hyperopia associated with severe cystic macular lesion with or without peripheral schisis, and subnormal ERG b-waves are findings more frequently reported at a very young age, while retinal detachment or progressive macular atrophy with or without peripheral retinal

scar, low visual acuity, and non-detectable ERG b-wave with reduced a-wave are instead mostly found in older ages. The OCT has been used to classify XLRS clinical severity. For example, clinical severity was determined by retinal examination and OCT scans in a cohort of 19 males, disregarding the genotype of the examined group (Prenner et al., 2006). Retinal tomography was more recently used (Lesch et al., 2008) to assess the prevalence of “cystic” and “atrophic” forms of the disease, variable with age. Visual acuity changes have been also considered valuable for predicting the extent of XLRS disease. However, Apushkin (Apushkin et al., 2005) analyzed the natural course of visual acuity changes in 38 XLRS patients, aged 9 to 65 years, finding only limited progression of vision loss over a mean follow-up period of 10 years.

Investigators have explored whether the type of mutations on the *RS1* gene predict the severity of the disease. More than 160 mutations have been identified in the *RS1* gene so far (1998). Mutations cause loss of protein function either due to the absolute loss of protein expression or to the presence of conformationally defective misfolded protein. The majority is missense mutations in exons 4–6; deletions, insertions, nonsense, and splice-site mutations have also been reported (Table 1). Several other studies have been conducted to ascertain correlations between genotype and phenotype in XLRS (Bradshaw et al., 1999; Eksandh et al., 2000a; Hiriyanna et al., 1999; Hotta et al., 2001; Lesch et al., 2008; Roesch et al., 1998; Shinoda et al., 2000; Sieving et al., 1999b); however, no clear link between genetic mutations and clinical phenotype have been firmly established. Furthermore, 145 unrelated XLRS families were examined in search of a correlation in severity of clinical phenotypes with the associated gene mutations (Hiriyanna et al., 1999). They found that mutations able to produce truncated RS1 protein (from deletions, splice-site and frame-shift mutations) are clearly related with severe phenotype.

Moreover three Japanese XLRS patients were described with retinal detachment or severe macular lesion and low visual acuity at a very young age; two of them harbored deletions of exon 1 or of the boundary region between exon 3 and intron 3 (Shinoda et al., 2000). The authors also reported (Shinoda et al., 2004) a progressive XLRS phenotype in two siblings harboring a deletion of RS1 exon 4 and summarized that severe cases of XLRS are usually associated with upstream deletions (exons 1–3) in the *RS1* gene which prevent the formation of functional mRNA (Hiriyanna et al., 1999; Shinoda et al., 2000), whereas the mild cases have relatively well preserved visual function and are usually associated with downstream deletions (exon 4). Two XLRS patients harboring “donor splice” mutation in exon 4, known to produce a null biochemical phenotype, with peripheral and central schisis, subnormal or non-detectable b-wave, and reduced a-wave, whereas another four patients, carrying missense mutations (R200C and R102W) resulted in more preserved ERG b-wave and almost normal retinal periphery with slight macular changes were reported (Bradshaw et al., 1999). We recently described (Vijayarathy et al., 2010) a considerable difference between the severe clinical phenotype in subjects harboring *RS1* null-protein signal-sequence mutations and the less compromised retinal function in XLRS patients carrying missense mutation. These findings suggest that mutations, like deletions and frame shifts that putatively cause protein truncation, result in greater clinical severity of the disease, even if there is no univocal classification system for XLRS. All these mutations related to a partial or full loss of protein suggests a severe XLRS phenotype, and therefore, might be unified in a one group of non-missense severe variants (Table 1).

Mutations	No ^a	DNA structure	Protein structure	Protein function
Missense	>110	Change a single nucleotide	Code for a different amino acid	Affects protein folding, sorting, loss of protein
Nonsense	9	Codes for a stop codon	Could truncate the protein	Full or partial loss-of-function
Splice site	16	A genetic mutation that inserts or deletes a number of nucleotides in the specific site at which splicing of an intron takes place during the processing of precursor messenger RNA into mature messenger RNA	The abolishment of the splicing site results in one or more introns remaining in mature mRNA	Production of aberrant proteins
Deletions	26	Delete one or more nucleotides in DNA	In-frame deletions or frameshifts	Full or partial loss-of-function
Insertions	4	Insert one or more nucleotides into DNA	In-frame deletions or frameshifts	Full or partial loss-of-function
Silent	6	Change a single nucleotide	Code for the same amino acid	Native-like protein

Table 1. Genetic mutations in X-linked retinoschisis and their role in protein structure/function. ^a<http://www.retina-international.org/sci-news/xlrsmut.htm>.

3. Molecular modeling, functional role and severity of pathogenic mutations in human XLR5

Genetic mutations often cause a change in protein expression. As described above several primary mechanisms might be responsible for the loss of RS1 function due to genetic mutations. The first mechanism is the misfolding of the discoidin domain, which changes the putative adhesive properties of the protein. Caused by missense mutations, RS1 misfolding might initiate formation of aberrant proteins in non-native conformation. The second mechanism is the defective disulfide-linked subunit assembly of RS1 into dimers and octamers which results in abnormal protein secretion caused by missense changes affecting reactive thiol groups. The third mechanism is the inability of RS1 to insert into endoplasmic reticulum (ER) membrane as part of the protein secretion process. This is caused by severe changes associated with the insertion or the removal of large fragments in protein molecule, protein truncations, and null mutations.

According to analysis in Paragraph 2.6 and Table 2 the majority of XLR5 mutations could be divided in two large groups of (a) missense mutations and (b) non-missense changes with a severe XLR5 phenotype. Although a severe role of non-missense changes is confirmed in numerous cases, the severity of XLR5 phenotype for missense changes is less obvious. Here we imply molecular modeling of protein structure as described by ERGs clinical severities of XLR5 via the computational evaluation of impact of pathogenic missense mutations.

3.1 Protein folding/misfolding in ER and protein folding landscapes

The effect of missense mutations on a protein fold is difficult to understand without some basics of the native protein folding. Over one-third of newly synthesized proteins are translocated into the ER, which ensures their delivery into the secretory pathway. The ER lumen contains molecular chaperones that maintain polypeptide solubility, enzymes that are necessary for post-translational modification of proteins, and factors that directly assist in the folding of newly synthesized polypeptides such as foldases and isomerases. Proteins that not attain their native conformations, because of genetic mutations, cellular stress or other random events, may harm the cell. Therefore, protein systems within the ER lumen mediate quality control, that resulting in the resolution of terminally misfolded proteins from correctly folded proteins and folding intermediates. To compensate for the potentially disastrous consequences of misfolded protein accumulation, ER-retained species are most commonly destroyed.

There are numerous observations of retinoschisis modified by missense mutations and expressed in cell culture which demonstrate the absence of modified RS1 bands from SDS-PAGE or native gels and associated with a loss of protein due to misfolding and rapid degradation (Wang et al., 2002; Wang et al., 2006; Wu and Molday, 2003; Wu et al., 2005). Several major mechanisms lead to degradation of misfolded protein. About 30% of cytosolic proteins carry specific KFERQ-targeting motifs in their sequences allowing for selective targeting of cytosolic proteins to the lysosome for degradation by chaperone-mediated autophagy (Kaushik and Cuervo, 2006, 2008). However, the absence of the specific targeting motif in the RS1 sequence suggests another option. As a result, misfolded or unassembled proteins are retained in the ER bound to chaperones or lectins until they are delivered to the cytosol for degradation in the ubiquitin-proteasome pathway (Goldberg, 2003). Mutant variants with significant changes in protein fold caused by missense mutations or deletions could generate misfolded proteins susceptible to hydrolysis similar to that of human haemoglobin in which about one-fifth of missense proteins undergo rapid degradation (Goldberg, 2003). Therefore, the severe mutant variants are expected to have a markedly perturbed non-native protein fold causing misfolding in the ER and later digestion in the proteasome (Vijayarathy et al., 2010).

The mechanism by which a polypeptide chain folds to a specific three-dimensional protein structure was recently discussed (Dobson, 2004). In the ER, proteins fold into their native conformations and undergo different post-translational modifications and the formation of disulphide bonds. Native states of proteins almost always correspond to the structures that are most thermodynamically stable under physiological conditions. The primary sequence of protein is the major determinant for proper folding of protein (Anfinsen et al., 1961). The protein folds along several competing pathways into intermediate, non-native structures with decreasing free energies until it achieves a conformation with the lowest energy to form a protein with native interactions (Dobson, 2004). The total number of possible conformations of any polypeptide chain is so large that a systematic search for this particular structure would be impractical. The folding process involves a random search of many protein folds accessible to a polypeptide chain.

The natural fluctuations in the conformation of an unfolded or incompletely folded polypeptide chain cause highly separated residues in the amino-acid sequence to come into contact with one other. In addition, if the energy surface of protein or 'landscape' has the correct shape, only a small number of all possible conformers needs to be tested by any given protein molecule during its transition from a random coil to a native structure. The

landscape is encoded by the amino-acid sequence of protein. Therefore, natural selection has enabled proteins to change so that polypeptides are able to fold rapidly and efficiently. Such a description is often referred to as the 'new view' of protein folding (Dobson, 1999, 2003, 2004). On average, native-like interactions between residues are more determined and the polypeptide chain is finding lowest-energy structure by a process of trial and error. Misfolded or intermediate non-native proteins never achieve this lowest energy minimum. Pathogenic mutations produce a severe or mild effect in a protein structure and cause the protein to stay in an intermediate or even misfolded conformation with a relatively higher free energy.

3.2 Role of cysteine residues and disulphide bonds in protein stability

Cysteine residues normally form disulphide bonds which significantly constrain the number of possible conformers from finding a lowest-energy structure. The disulphide bond or disulphide bridge is formed by the pairing of two thiol groups of cysteines as a result of protein oxidation. A disulfide bond is a strong covalent bond of about 2.05 Å in length connecting two sulfur S_V atoms which dissociate with energy of 60 kcal/mole. The structure of a disulfide bond can be described by its χ_{ss} dihedral angle between the $C^\beta - S_V - S_V - C^\beta$ atoms, which is in majority close to $\pm 90^\circ$. When the dihedral angle approaches 0° or 180° , then the disulfide is a better oxidant. Rotation about the $S_V - S_V$ axis has a low energy barrier.

The disulfide bond holds two fragments of the protein chain together. This stabilizes the native fold of a protein by lowering entropy of the polypeptide chain and by condensing hydrophobic residues around the bond into local hydrophobic core using hydrophobic interactions. The disulfide bond increases the effective local concentration of hydrophobic residues causing a decrease of the local concentration of water molecules in the hydrophobic core. Since water molecules break up hydrogen bonds, their low concentration stabilizes a protein secondary structure.

The native disulphide bonds are critical for proper protein folding. The native structure of a protein typically has a single disulfide bond. In proteins with more than two cysteines, non-native disulfide species may be created. Non-disulphide species are almost always unfolded. As the number of cysteines increases, the number of non-native species increases significantly. Indeed, RS1 monomer has 10 cysteines which can form up to five disulphide bonds. In general, 10 cysteine residues can form ${}_{10}C_2=45$ distinct disulphide bonds. A protein with ten-cysteines, such as RS1, could form 945 $[=10!/(10/2)!2^{10/2}]$ different five-disulfide species, only one of which is the protein with native disulfide bonds. All other 944 proteins are the non-native disulphide species!

In the cell in order to avoid non-native disulphides formation, protein disulphide isomerases (PDI) are necessary to catalyze the inter-conversion of disulfide species and accelerate the formation of the native disulfide species. In the ER, PDI has a function of a cellular chaperone with the essential foldase activity to maintain a native protein fold (Noiva, 1999; Tsai et al., 2001). PDI catalyzes oxidation and reshuffling (isomerization) of disulphides in substrate proteins by using the catalytic CxxC motif (Gruber et al., 2006). Current data suggest that PDI docks close to two S_V cysteines in the substrate protein, forms a native disulphide bridge between those cysteines, and possibly stabilizes native contacts in that area by utilizing a chaperone function. Thus, we might conclude that PDI's are an essential interaction partners of RS1 in ER in order to form a structure with native disulphide bonds.

Hence, we suggest that genetic mutations which are associated with the cysteine insertion/removal might interfere with suitable PDI binding in the vicinity of missense change. This might cause the appearance of new non-native disulphide bonds previously corrected by the foldase action. The insertion or deletion of cysteine residues should be taken into account when the severity of damage to protein molecule caused by the pathogenic missense change is evaluated.

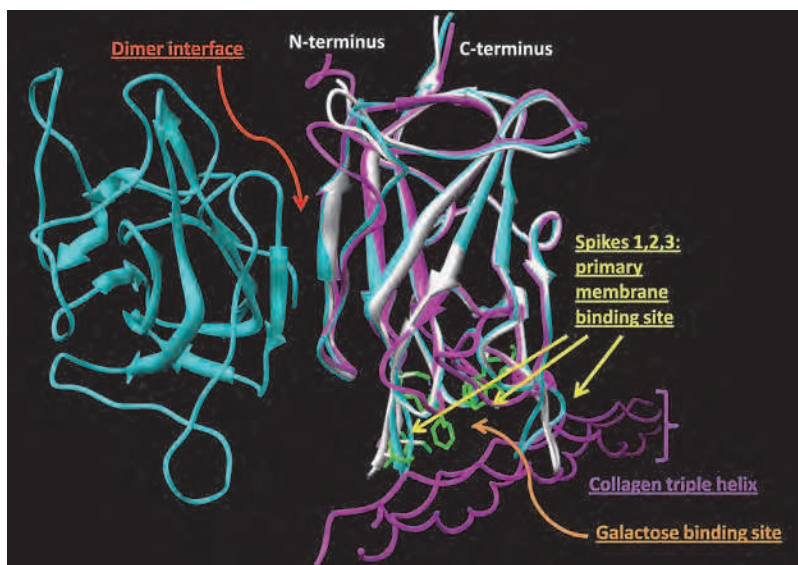


Fig. 3. A superposition of 3 discoidin ribbon structures to demonstrate the areas involved in interactions of discoidin domains with other molecules. Structures of the DDR2 discoidin domain bound to a triple-helical collagen peptide (magenta), the dimeric (cyan) and monomeric (white) forms of the membrane-binding C2 domain of human coagulation factor V (cyan) are shown.

3.3 Discoidin domains and molecular modeling of RS1 protein structure

Currently more than 72,000 protein structures have been determined by protein crystallography and deposited in the RCSB protein data bank. This list could be significantly expanded if structural genomic approaches such as a sequence homology and molecular modeling are used to generate protein structures. These computational methods were used successfully to predict the effect of thermodynamics experiments, to simulate the dynamics of protein folding and unfolding, and to explain a functional and structural role of elements of protein structure and other areas.

Similar methods could be used to evaluate an impact of missense mutations on protein structure stability and function. We used molecular modeling to predict a structure of mature retinoschisin which is formed by Rs1 and discoidin domains (Sergeev et al., 2010). Discoidin domains have a similar fold with elements of spatial structure in a shape of a β -sandwich, shown schematically in Figure 3 (Baumgartner et al., 1998) as the superposition of three structures demonstrating a binding to different molecules. The galactose,

phospholipids, and collagen binding sites are located in shown in the lower part of this figure (area of spikes) suggesting a high conformational flexibility in this area (Carafoli et al., 2009; Macedo-Ribeiro et al., 1999). Moreover, the discoidin domains are able to form a dimeric structure shown by the cyan ribbon (Macedo-Ribeiro et al., 1999). Therefore binding to galactose, membrane, collagen, and a dimer formation could be potentially expected for the discoidin domain of retinoschisin. In general, the discoidin fold is conserved in more than 9 different proteins. The discoidin domain is present in single or multiple copies in extracellular or trans-membrane proteins implicated in cell-cell adhesion, and cell-cell interaction such as the coagulation factors V (FaV) and VIII (FaVIII), milk fat globule, neuropilin and neurexins, and implicated in phospholipid binding (Adams et al., 2004). In different species they have 47 highly conserved residues (~30% sequence identity) including 2 cysteines forming a disulphide bridge and several tryptophans maintaining a stable hydrophobic core of a discoidin domain β -sandwich (Kiedziarska et al., 2007). The structure of mature retinoschisin is shown in Figure 4A. In this structure the Rs1 domain is located in residues 25-64 and the folded, β -sandwich discoidin domain occupies residues 65-224 (Wu and Molday, 2003). The structure of the mature retinoschisin was equilibrated using molecular dynamics (MD). Usually MD is used to obtain an 'idealized' or equilibrated protein structure with stereochemistry close to perfect. The main justification of the MD method is that statistical ensemble averages are equal to time averages of the system, so-called the ergodic hypothesis. MD by computer simulation of physical movements by atoms and molecules take into account physical interactions between atoms of the protein structure and molecules of surrounding waters. Whereas it is possible to take "still snapshots" of crystal structures using X-Ray crystallography and NMR, no current experimental technique allows access to all the time scales of motion at atomic resolution.

MD can be used to refine the location of cysteine residues in the RS1 structure which is necessary to understand retinoschisin function (Wang et al., 2002; Wang et al., 2006; Wu and Molday, 2003; Wu et al., 2005). The structure of mature RS1 contains 10 cysteines in positions 38, 40, 42, 59, 63, 83, 110, 142, 219, and 223, which are shared in an even proportion between Rs1 and discoidin domains (Figure 4A). The structure of the discoidin domain and the positions of 5 cysteines were reported in several cases (Fraternali et al., 2003; Wang et al., 2006; Wu and Molday, 2003). The other 5 cysteines are located in the Rs1 domain of mature retinoschisin. In a protein structure, 7 cysteines are predicted to be concentrated in an area close to amino- and carboxy-termini, and 3 cysteines are located close to a spike area shown at the top (terminal extensions) and the bottom (discoidin domain) parts of Figure 4A, respectively. Nearly 70% of the RS1 surface is formed by non-polar groups (see Figures 4B and C, rotation of $\sim 180^\circ$) suggesting that non-polar groups (green) could be important for the RS1 normal function.

Although numerous experiments have demonstrated that retinoschisin is secreted as a monomer, dimer, or octamer in model cell systems (Wang et al., 2006; Wu et al., 2005) this protein is secreted *in vivo* as a homo-oligomeric complex. A structural model of secreted RS1 homo-oligomeric protein complex currently is not available. Oligomerization is critical for the functioning of retinoschisin as an extracellular adhesion protein (Wu et al., 2005) where non-polar surface of RS1 could play a role. In contrast, protein misfolding caused by pathogenic mutation could interrupt proper secretion of a functional protein (Wang et al., 2002; Wang et al., 2006; Wu and Molday, 2003).

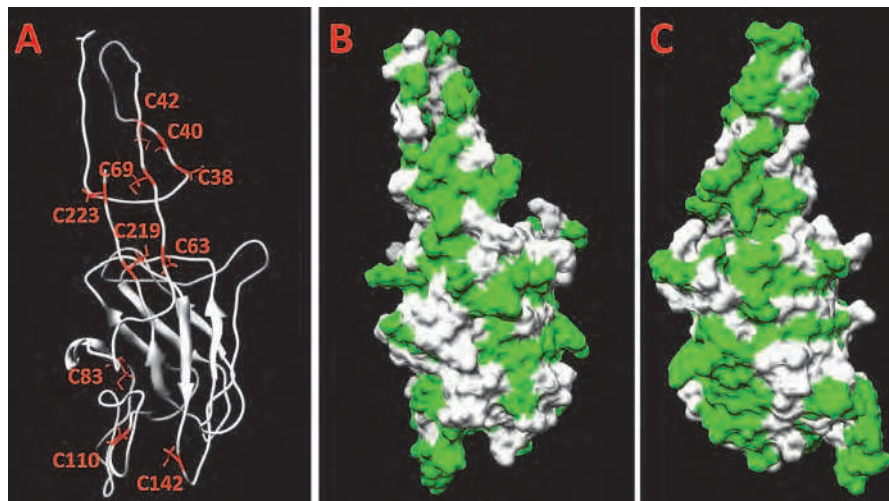


Fig. 4. RS1 structure is a monomer with a significant fraction of non-polar surface. RS1 structure is shown by a ribbon (Panel A). Positions of cysteines are shown in red. Accessible surface area of RS1 demonstrates a significant proportion of exposed non-polar areas shown by green (Panels B and C).

3.4 Computational assessment of severity of protein damage caused by the pathogenic missense change

in the last decade, new approaches using semi-empirical force-fields were developed in molecular modeling. Stability of native protein structure and protein complexes is defined by non-polar interactions, disulphide covalent bonds, salt bridges, and hydrogen bonds. Semi-empirical methods imply simplified forces and potentials are taken into account for these interactions within protein structure. Semi-empirical methods generate values of protein stabilization energies that correlate well with an experimental data for a majority of tested proteins. This approach might help to grade severities of molecular perturbations due to missense changes and explain how a genetic mutation could impact protein structure in quantitative manner.

The free energy of protein stabilization (in kcal mol⁻¹) is a function of several parameters. The first term includes a solvation energy contribution from hydrophobic and polar groups of protein (Eisenberg and McLachlan, 1986) based on a concept of accessible surface area (Lee and Richards, 1971) which could be evaluated using a fast geometry algorithm (Tsodikov et al., 2002). The second term is the energy of hydrogen bonds with regard to simple geometric considerations (Petukhov et al., 1999). Additional terms include Van der Waals energy which takes into account the experimental transfer energies from water to vapor; the electrostatic coulomb free energy term, which describes electrostatic interactions in protein; the crude entropy of protein chain to obtain a measure of free energy and free energy of the steric overlaps between atoms in protein structure (Abagyan and Totrov, 1994; Munoz and Serrano, 1994).

Currently, all these terms are combined in the FoldX force field (Schymkowitz et al., 2005; Schymkowitz et al., 2002). The rapid evaluation of protein stabilization free energy change

due to missense mutations could be accessed with this field based on an empirical energy function derived from experimental work on proteins. The predictive power of this approach has been successfully tested with experimental thermodynamics data of 1000 mutant proteins (Guerois et al., 2002) from the ProTherm database (Gromiha et al., 2000; Gromiha et al., 1999; Gromiha et al., 2002). Recently a combination of molecular dynamics folding simulations and FoldX potential has been suggested as an approach of *in silico* analysis of missense substitutions (Tavtigian et al., 2008). In our work, the changes in energy of protein stabilization due to missense change were evaluated using semi-empirical methods using the FoldX force field.

In addition, we used information about differences between amino acids replacing each other in order to achieve a correct estimate for mutations involving cysteine residues. The amino acids differ by combination of several chemical factors like composition, polarity and molecular volume which correlate best with protein residue substitution frequencies as observed (Grantham, 1974). The Grantham difference for each amino acid pair could be used to characterize a physiochemical differences between wild-type and missense variant amino acid residues (Karchin et al., 2007; Tavtigian et al., 2008).

Therefore, we suggested a molecular grading scale, so-called a computed impact score, *CI* (Sergeev et al., 2010), which considers changes in protein conformation and the Grantham differences between amino acids. Graphically, with these two categories as axes, the computed impact shows the characteristic distance between two amino acids involved in the mutation change. The axes are made orthogonal to facilitate the calculation of the difference in distance between amino acids. The overall difference, which is described by the *CI*, demonstrates the overall difference between two amino acids for the same position in wild-type protein and mutant variant. The changes in energy of protein stabilization, $\Delta\Delta G_{stab}$, the *CI*, and accessible surface areas, ASA, were determined in our XLRS cohort, as shown in Table 2 for several mutations. Finally, the computed impact score used to grade an impact of each pathogenic mutation at the protein level was compared with severity of XLRS estimated from ERG data.

Missense mutation	$\Delta\Delta G_{stab}$, kcal/mol	CI	ASA, Å ²	Missense mutation	$\Delta\Delta G_{stab}$, kcal/mol	CI	ASA, Å ²
E72K	12.7	0.24	102	R141C	19.8	0.54	48
W92C	20.7	0.61	209	N179D	21.6	0.36	8
R102W	12.8	0.32	41	R200C	16.1	0.50	53
L127P	27.7	0.50	6	R213W	12.6	0.32	0
I136T	22.2	0.42	0	R213Q	10.6	0.20	0
G140E	12.1	0.30	0	C219W	3.9	0.52	4

Table 2. Computed impact, surface accessibility and protein stabilization energy change caused by the pathogenic missense mutations selected from our XLRS cohort. ASA is characterizing the residue exposure ($>40 \text{ \AA}^2$) or location in the protein hydrophobic core ($\leq 40 \text{ \AA}^2$).

3.5 Molecular grading scale: protein structure-based classification of the pathogenic missense mutations impact in human XLRS

We applied molecular modeling of the RS protein and consider perturbations caused by mutations found in human XLRS affected subjects. Computational analysis has predicted

that pathogenic missense mutations could be separated in two groups by using the molecular grading scale.

The ERG b/a-wave ratios were sorted by patient age and by the impact of mutation on protein atomic structure. This analysis was applied independently to ERG b/a-wave ratios as a function of average patient age versus severity of XLR5 phenotype (Figure 5A). To minimize the effect of statistical errors and to improve a signal-to-noise ratio in experimental ERG data, we used the method described previously (Sergeev et al., 2010) to a new XLR5 cohort of patients. All b/a-wave ratios were divided into groups by age (younger, older) and by mutation severity (low-impact, high-impact) (Figure 5A). The b/a-wave ratio in older (37-43 y/o) XLR5 patients was greater than younger (13-17 y/o) for severe missense variants with the b-wave unchanged as the a-wave declined similarly to that observed in the *Rslb-KO* mouse (Kjellstrom et al., 2007b) and in the NEI dataset (Sergeev et al., 2010). In the mouse model, the decline of a-wave amplitude with age coincided with the loss of outer nuclear layer cells, whereas the decline in the b-wave and the b/a-wave ratio was associated with increasing severity of schisis cavities in younger ages (Kjellstrom et al., 2007a). As result, phenotypic b/a-wave ratios declined for younger individuals accompanied by a corresponding rise of computed impact score, a measure of the structural severity of the mutation (Figure 5A). Although this change is statistically less significant for older patients, a common trend showing a slight decrease with computed impact seems to be similar to that of described for younger individuals.

Differences in phenotypes were verified for low- and high-impact missense changes and severe non-missense mutations (Figure 5B). Low-impact missense changes show average b/a-wave ratio close to 1.0 for a maximum with 15 XLR5 patients of different ages (labeled by star in bottom panel). This ratio corresponds to a maximum of 10 patients with an average value of approximately 0.6, which is consistent with more severe XLR5 phenotype as expected for high-impact missense variants. In addition, the severity of high impact missense changes is confirmed by identical correspondence to 15 patients with the severe non-missense variants (top panel). Thus, low- and high-impact missense changes in protein structure might be associated with mild and severe changes in the XLR5 phenotype.

Earlier we demonstrated that maximum structure perturbations associated with severe XLR5 phenotype arise from either the removal or insertion of cysteine residues or from changes in the hydrophobic core (Sergeev et al., 2010). Less severe or mild changes were associated with missense mutations targeting a significant part of protein surface. Our present study, which uses different datasets, has demonstrated that mild phenotypic changes could be associated with mutations in the water inaccessible residues when polar-to-polar or the hydrophobic-to-hydrophobic changes has appeared.

Our computational analysis has predicted that pathogenic missense mutations could be separated in mild and severe groups of XLR5 phenotype by using the molecular grading scale. The results for the expected phenotypes of 109 missense changes which are currently available for XLR5 are shown in the Table 3. In order to understand how the phenotype of XLR5 disease described by b/a-wave ratios is related to missense changes, we analyzed mutant residue accessibilities (ASA) in the RS1 structure similar to that of shown in the Table 2. All mutations were ranked according to their computed impact. These mutations were separated into two groups, low-impact and high-impact, by their computed severity threshold (~0.4) as previously demonstrated (Sergeev et al., 2010). From this analysis, half of the mild mutations could be considered as mutations which were partially or fully exposed

at the protein surface; another half are the mutations predicted to be buried in the hydrophobic core. Mutations from this latter group were variants related to insertion, exchange, or removal of charged residues or replacement with a homologous hydrophobic or polar residue. In only two cases, C223S and C83S, cysteines were affected by a mild missense change. In contrast, the majority of missense variants were predicted to cause severe changes, related to insertion or removal of cysteine residues (23 mutations) and/or buried in the hydrophobic core.

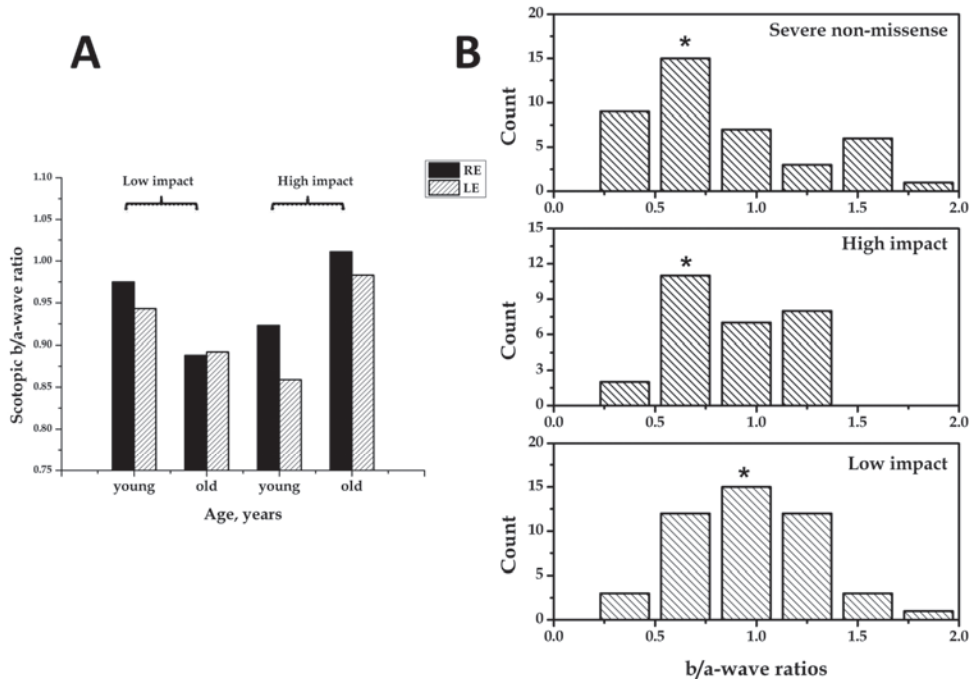


Fig. 5. Severity of the XLRS phenotype is associated with the expected impact of missense changes on the RS1 protein structure. **Panel A:** ERG average b/a-wave ratios as a function of average patient age and severity of XLRS phenotype. Average b/a-wave ratios obtained for patients divided into 4 groups by missense mutations classes (low-impact, high-impact) and by patient age (young, old). Scotopic b/a-wave ratios for 4 groups of patients are shown. ERG b/a-wave ratios for right (RE) and left (LE) eyes in each group are black and shaded, respectively. **Panel B:** Histogram of the XLRS patient b/a-wave ratios divided in groups of a low- and a high-impact missense, and severe non-missense genetic mutations as predicted using by a molecular grading scale. No differences in age were considered in this case. Histograms bars with maximum counts are labeled by asterisks (*). The ratios were obtained for the same XLRS cohort of patients (< 55 years old).

XLRS phenotype	Missense variants ^{a)}
Mild	R209H, D158N, R213Q, S73P, E146D, G70S, T185K, H207Q, I133F, A101P, R141H, E72K, G178D, E72D, Q154R, D168H, L113F, H207D, E72Q, E146K, G70A, A211T, G109A, R200H, R209L, E215Q, G109E, G140E, K167N, H222N, N104K, R141G, R102Q, R213W, R102W, P203L, T138A, P192A, A98E, G109R, C223S, W96R, P192T, I199T, P193L, R191P, C83S, A211F, P192S, R102E, E215K, D145H, P192R
Severe	C59S, R197P, G70R, I195V, P192L, N179D, L69P, R197H, V76G, G74V, G135V, G140R, L137P, R209P, L216P, R209G, E72A, P193S, R156G, E215V, C219S, I136T, D143V, P68R, C142R, G109W, C110R, L103R, Y89C, F176S, C223R, C110Y, C219G, R209C, N99C, R200C, L127P, R197C, G70D, C219W, R182C, C219R, R141C, W163C, W122C, Y65C, W112C, Y155C, I81N, I81D, W92C, W96C, F108C, C142W, C223Y

Table 3. Classes of XLRS phenotypes as predicted using the molecular grading scale for 110 pathogenic missense variants. ^{a)} Human Gene Mutation, Retina News International, and X-linked Retinoschisis Sequence Variation databases were used.

Finally, this study confirms results of our previous work that severe phenotype maximum structure perturbations are related to dramatic changes in a protein hydrophobic core or to the deletion or insertion of cysteine residues affecting in general the stability of protein fold. The kinetics of the disease progression might depend on the degree of the mutation impact on protein stability caused by the pathogenic missense change. Thus, we have to incorporate age, genotype, and molecular modeling into ERG analysis to understand a functional role of pathogenic mutations.

4. Incorporating age and genotype into ERG analysis

In our study, the effect of high-impact missense mutations could be recognized as severe at an earlier age when compared to low-impact missense mutations. In order to recognize the predicted affect of mutations we look to kinetics of the disease progression and incorporate patient age into the analysis of the relationship between genotype and phenotype. An exact understanding of how XLRS disease progresses with age is not clear. A 15-year, longitudinal XLRS study suggests that XLRS is a more stationary disease up to age 35 years, as seen in baseline and follow up ERG testing of 10 subjects. The first examination was performed on subjects between 6 to 15 years of age. A follow up examination was preformed 8 to 14 years later. In both exams, all 10 subjects showed reduced b-wave amplitudes, and no difference was found between the b-wave amplitude of the first or second visit (Kjellstrom et al., 2010). With these studies in mind, we raised the question of what role XLRS mutation severity plays in the dark-adapted ERG response. We preformed a retrospective cross-sectional study on 73 XLRS subjects who were seen at the National Eye Institute between 2004 and 2010. All subjects underwent ocular examination including a full-field ERG with ISCEV standard, dark-adapted response. All subjects were genotyped for *RS1* mutations. By separating subjects into two mutation severity groups (low-impact, high-impact), our data suggest that null protein or severity dysfunctional protein is associated with more retinal dysfunction than mildly dysfunctional protein. Greater dysfunction of subjects with severe

mutations was seen in the b-wave amplitude and b/a-wave ratio (70.2 μV , $p = 0.02$, less severe = 54 eyes, more severe = 79 eyes; excluding those >55 y/o). In our XLRS cohort, subjects maintained a-wave amplitudes within normal limits, or slightly below normal limits, suggesting little to no change in photoreceptor number or function in older subjects compared to younger subjects. Also, mutation severity did not play a role in a-wave amplitude (more severe $n = 44$ subjects, less severe $n = 30$, difference = -2.29 μV , $p=0.89$, excluding those >55 y/o). This data suggest that the outer segment of the photoreceptor was only minimally affected at most, and that mutation burden lies at the level of the photoreceptor-to-bipolar cell synapse.

Our cohort also displayed an earlier aging effect due to mutation than what would be expected from aging alone. The rise and fall of the b-wave amplitude with age in normal populations has been thoroughly studied (Birch and Anderson, 1992). At birth, the maximum response is minimal, but increases approximately 5 fold by age 4 months. By 5 years of age, children have normal adult b-wave amplitudes. The b-wave was not statistically affected from 5 years to 55 years of age, showing less than 25 μV decline per decade. Between ages 45-55 and 55-65, a significant decline of approximately 100 μV b-wave amplitude was seen. Birch's study showed that subjects ages 68 years have b-wave amplitudes approximately half those of subjects between the ages of 15 to 24 years.

For some time, investigators have questioned the possibility of photoreceptor disease in XLRS. One study found decreased a-wave amplitudes in 1/3 of their XLRS cohort, suggesting that rod photoreceptor dysfunction or loss could be a more primary manifestation of XLRS than first thought (Bradshaw et al., 1999). However, the majority of studies suggest complete or relative preservation of the a-wave in XLRS (Eksandh et al., 2000b; Kellner et al., 1990; Peachey et al., 1987). To look further into the question, Khan et al. modeled the leading edge of the a-wave to assess for pathology in the photo-transduction pathway (Khan et al., 2001). By modeling the first 15 ms of the waveform Khan found no difference between XLRS and normal subjects in sensitivity (S) and photoreceptor maximum amplitude (K_{max}) in the majority of XLRS waveforms measured.

4.1 The b/a-wave ratio can be a useful tool to quantify rod bipolar cell dysfunction relationship to rod function

To account for any compromise of the photoreceptor layer in XLRS, a ratio of photoreceptor-to-bipolar cell synaptic transmission compared to photo-transduction quality can be used (b/a-wave ratio). One can use the b/a-wave ratio to adjust for any photoreceptor dysfunction affect on the b-wave amplitude and can amplify the quantity of dysfunction in bipolar cells.

A reduced b/a-ratio is a characteristic of XLRS. The clinical lower limit of normal for the b/a ratio is 1.2 (Sergeev et al., 2010). Given normal b-wave amplitudes previous discussed, one would expect preservation of b/a-ratios in normal subjects until approximately 55 years of age (Birch and Anderson, 1992). In our study, no change in b/a ratio was due to aging alone ($n=143$ eyes, difference = 0.0039/year, $p=0.17$; excluding those >55 y/o); however, subjects with low-impact mutations maintained an overall higher b/a-ratio up to 55 years of age than did subjects with high-impact mutations (difference 0.3, $p = 0.005$, less severe = 54 eyes, more severe = 79 eyes; excluding those >55 y/o; Figure 6).

At first glance, it might appear that our study contradicts the XLRS longitudinal study by Kjellstrom (2010). However, had the longitudinal study identified the genetic mutations of all subjects (only three subjects were genotyped), a decrease in b/a-ratio could have been

expected in subjects with severe mutations. Of the three subjects who underwent genotyping, two had severe mutations and had decreased b/a-wave ratio at the follow up visit (ratios decreased from 1.2 to 0.8, and 1.1 to 0.77). According to our data, subjects with low-impact mutations would have only a modest change within the 10 to 15 year followup period.

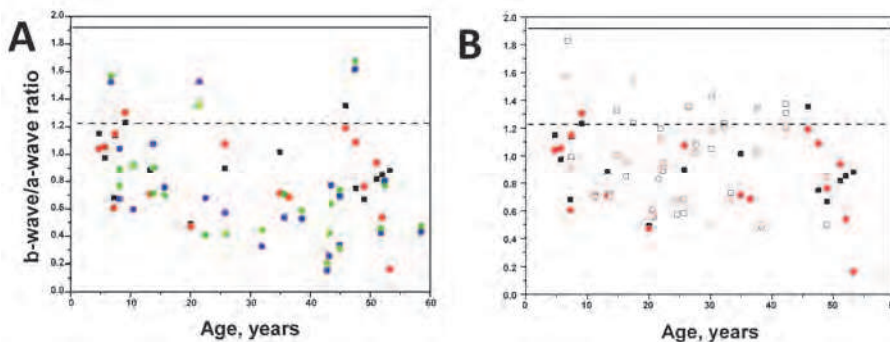


Fig. 6. Phenotypic data on clinical ERG b/a-wave ratios are shown for the cohort of X-linked retinoschisis patients as a function age (0-60 years old). Panel A: a superposition of ERG's b/a-wave ratios for patients with severe non-missense and high-impact missense variants. Panel B: a superposition of ERG's b/a-wave ratios for patients with the high-impact missense and low-impact missense variants. All data colored according to predicted severity: solid blue squares and green circles, solid black squares and red circles, open black squares and red circles are severe non-missense, high-impact missense and low-impact missense mutations. Squares and circles stand for right (OD) and left (OS) eye, respectively. The solid line and short dashes shows mean b/a-wave ratio and the mean minus two standard deviations, respectively, calculated from a group of 96 normal individuals (Sergeev et al., 2010).

5. Conclusion

Our computational analysis has suggested that the disease risk assessment at the atomic level could be implied in clinical studies. The combination of clinical electrophysiology, biology of retinal disease and molecular modeling provide a useful approach for evaluation of possible associations between the predicted structural alteration and/or damage to retinoschisin and the severity of XLRS disease.

6. Acknowledgment

We thank Sean Finnegan from the National Eye Institute for his valuable editorial help.

7. References

The Retinoschisis Consortium. (1998). Functional implications of the spectrum of mutations found in 234 cases with X-linked juvenile retinoschisis. *HumMolGenet* 7, 1185-1192.

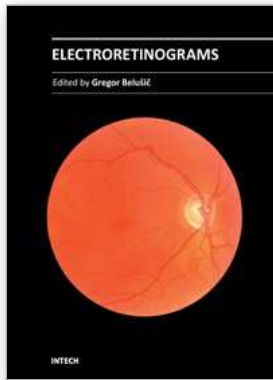
- Abagyan, R., and Totrov, M. (1994). Biased probability Monte Carlo conformational searches and electrostatic calculations for peptides and proteins. *J Mol Biol* 235, 983-1002.
- Adams, T.E., Hockin, M.F., Mann, K.G., and Everse, S.J. (2004). The crystal structure of activated protein C-inactivated bovine factor Va: Implications for cofactor function. *ProcNatlAcadSciUSA* 101, 8918-8923.
- Anfinsen, C.B., Haber, E., Sela, M., and White, F.H., Jr. (1961). The kinetics of formation of native ribonuclease during oxidation of the reduced polypeptide chain. *ProcNatlAcadSciUSA* 47, 1309-1314.
- Apushkin, M.A., Fishman, G.A., and Rajagopalan, A.S. (2005). Fundus findings and longitudinal study of visual acuity loss in patients with X-linked retinoschisis. *Retina* 25, 612-618.
- Baumgartner, S., Hofmann, K., Chiquet-Ehrismann, R., and Bucher, P. (1998). The discoidin domain family revisited: new members from prokaryotes and a homology-based fold prediction. *Protein Sci* 7, 1626-1631.
- Birch, D.G., and Anderson, J.L. (1992). Standardized full-field electroretinography. Normal values and their variation with age. *Arch Ophthalmol* 110, 1571-1576.
- Bradshaw, K., George, N., Moore, A., and Trump, D. (1999). Mutations of the XLR51 gene cause abnormalities of photoreceptor as well as inner retinal responses of the ERG. *DocOphthalmol* 98, 153-173.
- Breton, M.E., Schueller, A.W., Lamb, T.D., and Pugh, E.N., Jr. (1994). Analysis of ERG a-wave amplification and kinetics in terms of the G-protein cascade of phototransduction. *Invest OphthalmolVisSci* 35, 295-309.
- Carafoli, F., Bihan, D., Stathopoulos, S., Konitsiotis, A.D., Kvensakul, M., Farndale, R.W., Leitinger, B., and Hohenester, E. (2009). Crystallographic insight into collagen recognition by discoidin domain receptor 2. *Structure* 17, 1573-1581.
- Dobson, C.M. (1999). Protein misfolding, evolution and disease. *Trends BiochemSci* 24, 329-332.
- Dobson, C.M. (2003). Protein folding and misfolding. *Nature* 426, 884-890.
- Dobson, C.M. (2004). Principles of protein folding, misfolding and aggregation. *SeminCell DevBiol* 15, 3-16.
- Eisenberg, D., and McLachlan, A.D. (1986). Solvation energy in protein folding and binding. *Nature* 319, 199-203.
- Eksandh, L., Andreasson, S., and Abrahamson, M. (2005). Juvenile X-linked retinoschisis with normal scotopic b-wave in the electroretinogram at an early stage of the disease. *Ophthalmic Genet* 26, 111-117.
- Eksandh, L.C., Ponjavic, V., Ayyagari, R., Bingham, E.L., Hiriyan, K.T., Andreasson, S., Ehinger, B., and Sieving, P.A. (2000a). Phenotypic expression of juvenile X-linked retinoschisis in Swedish families with different mutations in the XLR51 gene. *Arch Ophthalmol* 118, 1098-1104.
- Eksandh, L.C., Ponjavic, V., Ayyagari, R., Bingham, E.L., Hiriyan, K.T., Andreasson, S., Ehinger, B., and Sieving, P.A. (2000b). Phenotypic expression of juvenile X-linked retinoschisis in Swedish families with different mutations in the XLR51 gene. *ArchOphthalmol* 118, 1098-1104.
- Eriksson, U., Larsson, E., and Holmstrom, G. (2004). Optical coherence tomography in the diagnosis of juvenile X-linked retinoschisis. *Acta Ophthalmol Scand* 82, 218-223.
- Forsius, H., Krause, U., Helve, J., Vuopala, V., Mustonen, E., Vainio-Mattila, B., Fellman, J., and Eriksson, A.W. (1973). Visual acuity in 183 cases of X-chromosomal retinoschisis. *Can J Ophthalmol* 8, 385-393.

- Fraternali, F., Cavallo, L., and Musco, G. (2003). Effects of pathological mutations on the stability of a conserved amino acid triad in retinoschisin. *FEBS Lett* 544, 21-26.
- Friedrich, U., Stohr, H., Hilfinger, D., Loenhardt, T., Schachner, M., Langmann, T., and Weber, B.H. The Na/K-ATPase is obligatory for membrane anchorage of retinoschisin, the protein involved in the pathogenesis of X-linked juvenile retinoschisis. *Hum Mol Genet*.
- George, N.D., Yates, J.R., Bradshaw, K., and Moore, A.T. (1995). Infantile presentation of X linked retinoschisis. *BrJ Ophthalmol* 79, 653-657.
- George, N.D., Yates, J.R., and Moore, A.T. (1996). Clinical features in affected males with X-linked retinoschisis. *Arch Ophthalmol* 114, 274-280.
- Goldberg, A.L. (2003). Protein degradation and protection against misfolded or damaged proteins. *Nature* 426, 895-899.
- Grantham, R. (1974). Amino acid difference formula to help explain protein evolution. *Science* 185, 862-864.
- Gregori, N.Z., Berrocal, A.M., Gregori, G., Murray, T.G., Knighton, R.W., Flynn, H.W., Jr., Dubovy, S., Puliafito, C.A., and Rosenfeld, P.J. (2009). Macular spectral-domain optical coherence tomography in patients with X linked retinoschisis. *Br J Ophthalmol* 93, 373-378.
- Gromiha, M.M., An, J., Kono, H., Oobatake, M., Uedaira, H., Prabakaran, P., and Sarai, A. (2000). ProTherm, version 2.0: thermodynamic database for proteins and mutants. *Nucleic Acids Res* 28, 283-285.
- Gromiha, M.M., An, J., Kono, H., Oobatake, M., Uedaira, H., and Sarai, A. (1999). ProTherm: Thermodynamic Database for Proteins and Mutants. *Nucleic Acids Res* 27, 286-288.
- Gromiha, M.M., Uedaira, H., An, J., Selvaraj, S., Prabakaran, P., and Sarai, A. (2002). ProTherm, Thermodynamic Database for Proteins and Mutants: developments in version 3.0. *Nucleic Acids Res* 30, 301-302.
- Gruber, C.W., Cemazar, M., Heras, B., Martin, J.L., and Craik, D.J. (2006). Protein disulfide isomerase: the structure of oxidative folding. *Trends BiochemSci* 31, 455-464.
- Guerois, R., Nielsen, J.E., and Serrano, L. (2002). Predicting changes in the stability of proteins and protein complexes: a study of more than 1000 mutations. *Journal of Molecular Biology* 320, 369-387.
- Hagins, W.A., Penn, R.D., and Yoshikami, S. (1970). Dark current and photocurrent in retinal rods. *Biophys J* 10, 380-412.
- Hiriyanna, K.T., Bingham, E.L., Yashar, B.M., Ayyagari, R., Fishman, G., Small, K.W., Weinberg, D.V., Weleber, R.G., Lewis, R.A., Andreasson, S., *et al.* (1999). Novel mutations in XLR51 causing retinoschisis, including first evidence of putative leader sequence change. *Hum Mutat* 14, 423-427.
- Hotta, Y., Nakamura, M., Okamoto, Y., Nomura, R., Terasaki, H., and Miyake, Y. (2001). Different mutation of the XLR51 gene causes juvenile retinoschisis with retinal white flecks. *Br J Ophthalmol* 85, 238-239.
- Huopaniemi, L., Fellman, J., Rantala, A., Eriksson, A., Forsius, H., De La Chapelle, A., and Alitalo, T. (1999). Skewed secondary sex ratio in the offspring of carriers of the 214G > A mutation of the RS1 gene. *Ann Hum Genet* 63, 521-533.
- Jablonski, M.M., Dalke, C., Wang, X., Lu, L., Manly, K.F., Pretsch, W., Favor, J., Pardue, M.T., Rinchik, E.M., Williams, R.W., *et al.* (2005). An ENU-induced mutation in Rslh causes disruption of retinal structure and function. *Mol Vis* 11, 569-581.

- Karchin, R., Monteiro, A.N., Tavtigian, S.V., Carvalho, M.A., and Sali, A. (2007). Functional impact of missense variants in BRCA1 predicted by supervised learning. *PLoSComputBiol* 3, e26.
- Kato, K., Miyake, Y., Kachi, S., Suzuki, T., Terasaki, H., Kawase, Y., and Kanda, T. (2001). Axial length and refractive error in X-linked retinoschisis. *Am J Ophthalmol* 131, 812-814.
- Kaushik, S., and Cuervo, A.M. (2006). Autophagy as a cell-repair mechanism: activation of chaperone-mediated autophagy during oxidative stress. *MolAspects Med* 27, 444-454.
- Kaushik, S., and Cuervo, A.M. (2008). Chaperone-mediated autophagy. *Methods MolBiol* 445, 227-244.
- Kellner, U., Brummer, S., Foerster, M.H., and Wessing, A. (1990). X-linked congenital retinoschisis. *Graefes ArchClinExpOphthalmol* 228, 432-437.
- Khan, N.W., Jamison, J.A., Kemp, J.A., and Sieving, P.A. (2001). Analysis of photoreceptor function and inner retinal activity in juvenile X-linked retinoschisis. *Vision Res* 41, 3931-3942.
- Kiedziarska, A., Smietana, K., Czepczynska, H., and Otlewski, J. (2007). Structural similarities and functional diversity of eukaryotic discoidin-like domains. *BiochimBiophysActa* 1774, 1069-1078.
- Kjellstrom, S., Bush, R.A., Zeng, Y., Takada, Y., and Sieving, P.A. (2007a). Retinoschisin gene therapy and natural history in the Rslh-KO mouse: long-term rescue from retinal degeneration. *Invest Ophthalmol Vis Sci* 48, 3837-3845.
- Kjellstrom, S., Bush, R.A., Zeng, Y., Takada, Y., and Sieving, P.A. (2007b). Retinoschisin gene therapy and natural history in the Rslh-KO mouse: long-term rescue from retinal degeneration. *Invest OphthalmolVisSci* 48, 3837-3845.
- Kjellstrom, S., Vijayarathy, C., Ponjavic, V., Sieving, P.A., and Andreasson, S. (2010). Long-term 12 year follow-up of X-linked congenital retinoschisis. *Ophthalmic Genet* 31, 114-125.
- Lee, B., and Richards, F.M. (1971). The interpretation of protein structures: estimation of static accessibility. *J Mol Biol* 55, 379-400.
- Lesch, B., Szabo, V., Kanya, M., Somfai, G.M., Vamos, R., Varsanyi, B., Pamer, Z., Knezy, K., Salacz, G., Janaky, M., *et al.* (2008). Clinical and genetic findings in Hungarian patients with X-linked juvenile retinoschisis. *Mol Vis* 14, 2321-2332.
- Li, X., Ma, X., and Tao, Y. (2007). Clinical features of X linked juvenile retinoschisis in Chinese families associated with novel mutations in the RS1 gene. *Mol Vis* 13, 804-812.
- Macedo-Ribeiro, S., Bode, W., Huber, R., Quinn-Allen, M.A., Kim, S.W., Ortel, T.L., Bourenkov, G.P., Bartunik, H.D., Stubbs, M.T., Kane, W.H., *et al.* (1999). Crystal structures of the membrane-binding C2 domain of human coagulation factor V. *Nature* 402, 434-439.
- Molday, L.L., Wu, W.W., and Molday, R.S. (2007). Retinoschisin (RS1), the protein encoded by the X-linked retinoschisis gene, is anchored to the surface of retinal photoreceptor and bipolar cells through its interactions with a Na/K ATPase-SARM1 complex. *JBiolChem* 282, 32792-32801.
- Molday, R.S. (2007). Focus on molecules: retinoschisin (RS1). *ExpEye Res* 84, 227-228.
- Munoz, V., and Serrano, L. (1994). Intrinsic secondary structure propensities of the amino acids, using statistical phi-psi matrices: comparison with experimental scales. *Proteins* 20, 301-311.

- Newman, E.A., and Odette, L.L. (1984). Model of electroretinogram b-wave generation: a test of the K⁺ hypothesis. *J Neurophysiol* 51, 164-182.
- Noiva, R. (1999). Protein disulfide isomerase: the multifunctional redox chaperone of the endoplasmic reticulum. *Semin Cell Dev Biol* 10, 481-493.
- Peachey, N.S., Fishman, G.A., Derlacki, D.J., and Brigell, M.G. (1987). Psychophysical and electroretinographic findings in X-linked juvenile retinoschisis. *Arch Ophthalmol* 105, 513-516.
- Petukhov, M., Cregut, D., Soares, C.M., and Serrano, L. (1999). Local water bridges and protein conformational stability. *Protein Sci* 8, 1982-1989.
- Prenner, J.L., Capone, A., Jr., Ciaccia, S., Takada, Y., Sieving, P.A., and Trese, M.T. (2006). Congenital X-linked retinoschisis classification system. *Retina* 26, S61-S64.
- Reid, S.N., Akhmedov, N.B., Piriev, N.I., Kozak, C.A., Danciger, M., and Farber, D.B. (1999). The mouse X-linked juvenile retinoschisis cDNA: expression in photoreceptors. *Gene* 227, 257-266.
- Robson, J.G., and Frishman, L.J. (1995). Response linearity and kinetics of the cat retina: the bipolar cell component of the dark-adapted electroretinogram. *Vis Neurosci* 12, 837-850.
- Roesch, M.T., Ewing, C.C., Gibson, A.E., and Weber, B.H. (1998). The natural history of X-linked retinoschisis. *Can J Ophthalmol* 33, 149-158.
- Sauer, C.G., Gehrig, A., Warneke-Wittstock, R., Marquardt, A., Ewing, C.C., Gibson, A., Lorenz, B., Jurklics, B., and Weber, B.H. (1997). Positional cloning of the gene associated with X-linked juvenile retinoschisis. *Nat Genet* 17, 164-170.
- Schymkowitz, J., Borg, J., Stricher, F., Nys, R., Rousseau, F., and Serrano, L. (2005). The FoldX web server: an online force field. *Nucleic Acids Res* 33, W382-W388.
- Schymkowitz, J.W., Rousseau, F., and Serrano, L. (2002). Surfing on protein folding energy landscapes. *Proc Natl Acad Sci USA* 99, 15846-15848.
- Sergeev, Y.V., Caruso, R.C., Meltzer, M.R., Smaoui, N., MacDonald, I.M., and Sieving, P.A. (2010). Molecular modeling of retinoschisin with functional analysis of pathogenic mutations from human X-linked retinoschisis. *Hum Mol Genet* 19, 1302-1313.
- Shi, L., Jian, K., Ko, M.L., Trump, D., and Ko, G.Y. (2009). Retinoschisin, a new binding partner for L-type voltage-gated calcium channels in the retina. *J Biol Chem* 284, 3966-3975.
- Shinoda, K., Ishida, S., Oguchi, Y., and Mashima, Y. (2000). Clinical characteristics of 14 Japanese patients with X-linked juvenile retinoschisis associated with XLRs1 mutation. *Ophthalmic Genet* 21, 171-180.
- Shinoda, K., Ohde, H., Ishida, S., Inoue, M., Oguchi, Y., and Mashima, Y. (2004). Novel 473-bp deletion in XLRs1 gene in a Japanese family with X-linked juvenile retinoschisis. *Graefes Arch Clin Exp Ophthalmol* 42, 561-565.
- Sieving, P.A., Bingham, E.L., Kemp, J., Richards, J., and Hiriyan, K. (1999a). Juvenile X-linked retinoschisis from XLRs1 Arg213Trp mutation with preservation of the electroretinogram scotopic b-wave. *Am J Ophthalmol* 128, 179-184.
- Sieving, P.A., Bingham, E.L., Kemp, J., Richards, J., and Hiriyan, K. (1999b). Juvenile X-linked retinoschisis from XLRs1 Arg213Trp mutation with preservation of the electroretinogram scotopic b-wave. *Am J Ophthalmol* 128, 179-184.
- Stockton, R.A., and Slaughter, M.M. (1989). B-wave of the electroretinogram. A reflection of ON bipolar cell activity. *J Gen Physiol* 93, 101-122.

- Takada, Y., Fariss, R.N., Muller, M., Bush, R.A., Rushing, E.J., and Sieving, P.A. (2006). Retinoschisin expression and localization in rodent and human pineal and consequences of mouse RS1 gene knockout. *Mol Vis* 12, 1108-1116.
- Tavtigian, S.V., Greenblatt, M.S., Lesueur, F., and Byrnes, G.B. (2008). In silico analysis of missense substitutions using sequence-alignment based methods. *HumMutat* 29, 1327-1336.
- Tsai, B., Rodighiero, C., Lencer, W.I., and Rapoport, T.A. (2001). Protein disulfide isomerase acts as a redox-dependent chaperone to unfold cholera toxin. *Cell* 104, 937-948.
- Tsodikov, O.V., Record, M.T., Jr., and Sergeev, Y.V. (2002). Novel computer program for fast exact calculation of accessible and molecular surface areas and average surface curvature. *JComputChem* 23, 600-609.
- Vijayasathya, C., Sui, R., Zeng, Y., Yang, G., Xu, F., Caruso, R.C., Lewis, R.A., Ziccardi, L., and Sieving, P.A. (2010). Molecular mechanisms leading to null-protein product from retinoschisin (RS1) signal-sequence mutants in X-linked retinoschisis (XLRS) disease. *Hum Mutat* 31, 1251-1260.
- Vijayasathya, C., Takada, Y., Zeng, Y., Bush, R.A., and Sieving, P.A. (2007). Retinoschisin is a peripheral membrane protein with affinity for anionic phospholipids and affected by divalent cations. *Invest OphthalmolVisSci* 48, 991-1000.
- Vijayasathya, C., Ziccardi, L., Zeng, Y., Smaoui, N., Caruso, R.C., and Sieving, P.A. (2009). Null retinoschisin-protein expression from an RS1 c354del1-ins18 mutation causing progressive and severe XLRS in a cross-sectional family study. *Invest Ophthalmol Vis Sci* 50, 5375-5383.
- Wang, T., Waters, C.T., Rothman, A.M., Jakins, T.J., Romisch, K., and Trump, D. (2002). Intracellular retention of mutant retinoschisin is the pathological mechanism underlying X-linked retinoschisis. *HumMolGenet* 11, 3097-3105.
- Wang, T., Zhou, A., Waters, C.T., O'Connor, E., Read, R.J., and Trump, D. (2006). Molecular pathology of X linked retinoschisis: mutations interfere with retinoschisin secretion and oligomerisation. *BrJOphthalmol* 90, 81-86.
- Weber, B.H., Schrewe, H., Molday, L.L., Gehrig, A., White, K.L., Seeliger, M.W., Jaissle, G.B., Friedburg, C., Tamm, E., and Molday, R.S. (2002). Inactivation of the murine X-linked juvenile retinoschisis gene, *Rs1h*, suggests a role of retinoschisin in retinal cell layer organization and synaptic structure. *ProcNatlAcadSciUSA* 99, 6222-6227.
- Wu, W.W., and Molday, R.S. (2003). Defective discoidin domain structure, subunit assembly, and endoplasmic reticulum processing of retinoschisin are primary mechanisms responsible for X-linked retinoschisis. *JBiolChem* 278, 28139-28146.
- Wu, W.W., Wong, J.P., Kast, J., and Molday, R.S. (2005). RS1, a discoidin domain-containing retinal cell adhesion protein associated with X-linked retinoschisis, exists as a novel disulfide-linked octamer. *JBiolChem* 280, 10721-10730.
- Zeng, Y., Takada, Y., Kjellstrom, S., Hiriyanna, K., Tanikawa, A., Wawrousek, E., Smaoui, N., Caruso, R., Bush, R.A., and Sieving, P.A. (2004). RS-1 Gene Delivery to an Adult *Rs1h* Knockout Mouse Model Restores ERG b-Wave with Reversal of the Electronegative Waveform of X-Linked Retinoschisis. *Invest Ophthalmol Vis Sci* 45, 3279-3285.



Electroretinograms

Edited by Dr. Gregor Belusic

ISBN 978-953-307-383-5

Hard cover, 238 pages

Publisher InTech

Published online 09, August, 2011

Published in print edition August, 2011

Electroretinography (ERG) is a non-invasive electrophysiological method which provides objective information about the function of the retina. Advanced ERG allows to assay the different types of retinal receptors and neurons in human and animal models. This book presents contributions on the recent state of the ERG. The book is divided into three parts. The first, methodological part, reviews standard methods and normatives of human ERG, reports about the advanced spatial, temporal and spectral methods of stimulation in human ERG, and deals with the analysis of the multifocal ERG signal. The second part deals with the ERG in different diseases of the human visual system and in diabetes. The third part presents the ERG in the standard animal models of human retinal disease: mouse, rat, macaque and fruitfly.

How to reference

In order to correctly reference this scholarly work, feel free to copy and paste the following:

Yuri V. Sergeev, Kristen E. Bowles, Lucia Ziccardi and Paul A. Sieving (2011). Molecular Modeling of Protein Structure, Biology of Disease and Clinical Electroretinography in Human X-Linked Retinoschisis (XLRS), Electroretinograms, Dr. Gregor Belusic (Ed.), ISBN: 978-953-307-383-5, InTech, Available from: <http://www.intechopen.com/books/electroretinograms/molecular-modeling-of-protein-structure-biology-of-disease-and-clinical-electroretinography-in-human>

INTECH

open science | open minds

InTech Europe

University Campus STeP Ri
Slavka Krautzeka 83/A
51000 Rijeka, Croatia
Phone: +385 (51) 770 447
Fax: +385 (51) 686 166
www.intechopen.com

InTech China

Unit 405, Office Block, Hotel Equatorial Shanghai
No.65, Yan An Road (West), Shanghai, 200040, China
中国上海市延安西路65号上海国际贵都大饭店办公楼405单元
Phone: +86-21-62489820
Fax: +86-21-62489821

© 2011 The Author(s). Licensee IntechOpen. This chapter is distributed under the terms of the [Creative Commons Attribution-NonCommercial-ShareAlike-3.0 License](#), which permits use, distribution and reproduction for non-commercial purposes, provided the original is properly cited and derivative works building on this content are distributed under the same license.